

Absolute ozone absorption cross section in the Huggins Chappuis minimum (350–470 nm) at 296 K

J. L. Axson^{1,2}, R. A. Washenfelder^{2,3}, T. F. Kahan¹, C. J. Young^{2,3}, V. Vaida^{1,2}, and S. S. Brown³

¹Department of Chemistry and Biochemistry, University of Colorado, Campus Box 215, Boulder, CO 80309, USA

²Cooperative Institute for Research in Environmental Sciences, 216 UCB, University of Colorado, Boulder, CO 80309, USA

³Chemical Sciences Division, National Oceanic and Atmospheric Administration, 325 Broadway, Boulder, CO 80305, USA

Received: 3 June 2011 – Published in Atmos. Chem. Phys. Discuss.: 1 August 2011

Revised: 4 November 2011 – Accepted: 9 November 2011 – Published: 21 November 2011

Abstract. We report the ozone absolute absorption cross section between 350–470 nm, the minimum between the Huggins and Chappuis bands, where the ozone cross section is less than 10^{-22} cm². Ozone spectra were acquired using an incoherent broadband cavity enhanced absorption spectrometer, with three channels centered at 365, 405, and 455 nm. The accuracy of the measured cross section is 4–30%, with the greatest uncertainty near the minimum absorption at 375–390 nm. Previous measurements vary by more than an order of magnitude in this spectral region. The measurements reported here provide much greater spectral coverage than the most recent measurements. The effect of O₃ concentration and water vapor partial pressure were investigated, however there were no observable changes in the absorption spectrum most likely due to the low optical density of the complex.

1 Introduction

Weak spectral absorptions play an important role in the radiative transfer of the Earth's atmosphere and accurate measurements of these are necessary for satellite retrievals of atmospheric trace gases (Burrows et al., 1999a; Bogumil et al., 2003; Petropavlovskikh et al., 2011). It has recently been recognized that weak electronic features in the near-ultraviolet (UV), which are not well known, can be important for tropospheric radical production (Waschewsky et al., 1996; Matthews et al., 2005; Vaida, 2009). Ozone (O₃) plays a key role both chemically and radiatively throughout the atmosphere, acting as an absorber and blocker of harmful UV

radiation (<300 nm) in the stratosphere and as the dominant source of OH radicals through its UV photolysis. Therefore, it is essential to have accurate O₃ absorption cross sections for satellite and ground based retrievals of vertical O₃ profiles and total O₃ columns, as well as to correctly model atmospheric O₃ concentrations (Burrows et al., 1999a; Bogumil et al., 2003; Petropavlovskikh et al., 2011).

Although the strong bands of O₃ have been well characterized (see reviews by Orphal (2003) and Gratien et al. (2010)), the absorption minimum between the Huggins and Chappuis bands at 350–470 nm is less well known, particularly the minimum region near 390 nm. Measurement of the weak O₃ absorption cross-section has practical importance for two reasons. First, satellites use the adjoining Huggins and Chappuis bands for direct retrievals of O₃, relying on the strongly varying differential cross-section (see Kroon et al. (2011) and references therein). Second, quantifying weak O₃ absorptions is necessary for satellite retrievals of other trace gases in this spectral region. For example, at 404 nm O₃ and NO₂ cross-sections have been previously reported to be 1.49×10^{-23} cm² molecule⁻¹ (Fuchs et al., 2009) and 5.9×10^{-19} cm² molecule⁻¹ (Voigt et al., 2002) respectively. For an O₃ column abundance of 8×10^{18} molecules cm⁻² (~300 Dobson units) and an NO₂ column abundance of 4×10^{15} molecules cm⁻² (Burrows et al., 1999b), the optical extinctions of the two molecules are 1×10^{-4} and 2×10^{-3} , respectively, and the O₃ extinction is both structured and significant (5% at 404 nm) in comparison to that of NO₂. Furthermore, literature cross sections at 404 nm vary from 1.5×10^{-23} to 7×10^{-23} cm² molecule⁻¹, or 5 to 30% of the NO₂ column extinction for these conditions. More accurate O₃ measurements are therefore required across its absorption minimum.



Correspondence to: S. S. Brown
(steven.s.brown@noaa.gov)

Table 1. Measurements of O₃ absorption cross section between 350–470 nm.

Reference	Instrumental	Spectral Region (nm)	Spectral Resolution (nm)	Temp (K)	Cross section at 365 nm ($\times 10^{-23}$ cm ²)	Cross section at 405 nm ($\times 10^{-23}$ cm ²)	Cross section at 455 nm ($\times 10^{-22}$ cm ²)
	Technique						
Burkholder and Talukdar (1994) ¹	Grating spectrometer	410–760	0.20	298	–	–	1.82
Brion et al. (1998) ²	FTS	350–830	0.01	295	4.47	1.49	2.06
Burrows et al. (1999)	Grating spectrometer	231–794	0.2–0.3	293	6.26	4.27	2.29
Voigt et al. (2001)	FTS	230–851	0.027	293	7.81	7.19	2.24
Bogumil et al. (2003)	Grating spectrometer	230–1075	0.26	293	5.11	2.12	2.14
Fuchs et al. (2009) ¹	CRDS	404	0.5	–	–	1.49 ³	–
Chen and Venables (2011) ¹	IBBCEAS	335–375	0.26	296	4.92	–	–
This work	IBBCEAS	350–470	0.27–0.51	296	3.68	1.51	1.88

¹ λ_{air} converted to λ_{vacuum} using Ciddor (1996) Eq. (1). ² Wavelength scale not specified. ³ Cross-section reported at $\lambda_{\text{vacuum}} = 404.1$ nm.

Previous O₃ cross sections in this region have been measured using high resolution Fourier transform spectrometers (Brion et al., 1998; Voigt et al., 2001) and grating spectrometers (Burkholder and Talukdar, 1994; Burrows et al., 1999a; Bogumil et al., 2003). These studies report cross sections that differ by more than an order of magnitude near the minimum, and also show some disagreement where the cross section is greater (e.g. 8 % at 350 nm and 20 % at 450 nm). These studies have also shown that the spectra, with their large discrepancies, are highly temperature dependent (Brion et al., 1993; Burkholder and Talukdar, 1994; Burrows et al., 1999a; Voigt et al., 2001; Bogumil et al., 2003). Table 1 summarizes the results of prior studies, and gives their spectral range, spectral resolution, temperature, and measured cross sections. The importance of O₃ absorption in the atmosphere, and the large discrepancies in the current literature over a wide spectral region around the O₃ absorption minimum, highlight the need for more accurate measurements of these very weak absorption cross sections.

Incoherent broadband cavity enhanced absorption spectroscopy (IBBCEAS) is a recently developed, highly sensitive method to measure trace gases and weak absorption cross sections (Fiedler et al., 2003). IBBCEAS instruments consist of an intense broadband light source, such as an arc lamp or light emitting diode (LED), high-finesse optical cavity, and multichannel detector. The pathlength generated by the optical cavity can be several tens of kilometers, making IBBCEAS more sensitive than traditional spectroscopic techniques. This increased optical path length is balanced by a reduction in intensity throughput, such that the greatest sensitivity increase is realized for bright input light sources. This technique was first described in the literature by Fiedler et al. (2003), and has subsequently been used for spectroscopic measurements of NO₂, NO₃, CHOCHO, HONO, and other trace gasses (Venables et al., 2006; Langridge et al., 2006; Gherman et al., 2008; Langridge et al., 2008; Vaughan et al., 2008; Washenfelder et al., 2008; Thalman and Volkamer, 2010). More recently, Chen and Venables (2011) used an IB-

BCEAS with an arc lamp to measure the O₃ cross section in the near-UV from 335–375 nm.

In this investigation, an IBBCEAS instrument with three channels centered at 365, 405, and 455 nm was designed, constructed, and characterized to measure O₃ absorption cross sections in the region between the Huggins and Chapuis bands, from 350 to 470 nm. The increased sensitivity of this instrument compared to single-pass or multi-pass cells allows for the measurement of these weak absorption cross sections with higher signal-to-noise and accuracy. Calibrations are based on 253.7 nm absorption of O₃ (Hg line) and Rayleigh scattering cross sections of pure gases, as described below. Both analytical standards are known to high accuracy. These results are compared to the previous literature studies of O₃ cross sections in this region.

2 Experimental

2.1 Description of the IBBCEAS instrument

The IBBCEAS used to measure O₃ absorption cross sections from 350 to 470 nm is shown in Fig. 1a. Each channel consists of an LED, lenses, a cavity composed of high-reflectivity mirrors, and an optical filter. An optical fiber connects the spectral output to a grating spectrometer with a CCD array detector. Three cavities were required to span the range of interest for the O₃ minimum. The spectral bandwidth for any single cavity is defined both by the emission spectrum of the LED light source, the useful bandwidth of the high reflectivity mirrors, and any optical filtering requirements, as described below. The broadband radiation was supplied by LEDs centered at 365 nm (Nichia NCSU033A(T) UV LED), 405 nm (LedEngin, Inc., LZ1-00UA05) and 455 nm (LedEngin, Inc., LZ1-00DB05) powered by custom-built, constant current DC power supplies controlled at 0.5, 0.7, and 1.0 A respectively. Each LED was mounted on a temperature-controlled block with a servoed

thermoelectric cooler (Watlow, EZ-ZONE[®] PM) and maintained at 293 K. Radiation was collimated and coupled into each of the 100 cm long cavities using a 2" diameter F/1.2 lens. The cavities were formed using highly reflective mirrors (Advanced Thin Films) with 1 m radius of curvature. The center wavelengths and maximum reflectivities were 362 nm ($R=0.99975$), 405 nm ($R=0.99994$), and 455 nm ($R=0.99993$). In cavity enhanced absorption spectroscopy, the effective path length can be defined as equal to an e^{-1} decay of light from the cavity. From this definition, the effective path lengths were 4.0 km, 17 km, and 14 km respectively, when the three cavities contained pure helium (He). Apertures of 1.5 cm diameter were used at the entrance and exit of each cavity to prevent light transmission at the uncoated edges of the 2.5 cm cavity mirrors.

Upon exiting the cavity, the light passed through a quartz beam splitter that was used to turn the beam of a HeNe laser through the cavity for alignment purposes. A 1" F/3 lens collimated the exiting radiation onto an optical fiber. Bandpass filters on each of the optical fibers prevented stray light from entering the spectrometer. The center wavelength and full width at half maximum (FWHM) for the bandpass filters were 360 nm with FWHM of 50 nm (Omega Optical 360WB50); 400 nm with FWHM of 70 nm (Andover Corp. 400FS70-25) or 40 nm (ThorLabs, FB400-40); and 450 nm with FWHM of 40 nm (Thorlabs, FB450-40). The optical fibers were coupled to a fiber bundle that was input to a Czerny-Turner grating spectrometer with CCD detector (Acton InSpectrum 150), as described in detail by Washenfelder et al. (2008). The fiber bundle illuminated two separate regions of the CCD, allowing spectra from two independent channels to be measured simultaneously. The spectrometer was configured with a 20 μm slit width and 1200 groove/mm grating (500 nm blaze), giving a spectral range of ~ 117 nm. Spectra of the three channels covering the 350–470 nm spectral region were acquired in two separate experiments. The grating was rotated to give a useful spectral range from 331 to 451 nm while measuring the 365 nm and 405 nm channels, and a spectral range from 380 to 484 nm while measuring the 405 nm and 455 nm channels. The wavelength calibration of the spectrometer was determined using an Hg/Ar calibration lamp with vacuum wavelengths of 334.24, 404.77, 407.90, and 435.96 nm (Sansonetti et al., 1996), and is accurate within 0.5 nm. The fixed slit width of 20 μm was found to give a nearly Gaussian lineshape. Because the experiment used an imaging spectrometer to image the input light onto the CCD, the FWHM increased linearly with wavelength (but was constant in frequency space) for the two wavelength determinations. For the 365 nm and 405 nm cavity experiment, the FWHM was 0.27 nm at 350 nm and 0.51 nm at 430 nm. For the 405 nm and 455 nm cavity experiment, the FWHM was 0.29 nm at 380 nm and 0.50 nm at 470 nm.

The sample cells were cylindrical aluminum cells of 2.2 cm inner diameter centered on the optical cavities with ports for the introduction and exhaust of the sample gas. The

O₃ concentration entering and exiting the cells was measured and it was determined that there was no loss to the walls. In addition, there was no evidence of other features in the spectrum; only those of O₃ were observed. The ports were immediately adjacent to the end mirrors, such that there was no purge volume used between the mirrors and the sample, as has often been employed in previous field and laboratory IB-BCEAS and cavity ring down (CRDS) experiments (Brown et al., 2000; Dube et al., 2006). Mounts with 2.0 cm diameter graphite rods were used to stabilize the cavities. Temperature and pressure in the cavities were measured at the connection between the two IB-BCEAS cavities. A thermocouple monitored the temperature, which ranged from 295.1–295.8 K, and a transducer (Honeywell, PPT0015AXN5V) monitored pressure, which ranged from 820.7–830.8 hPa.

2.2 Ozone generation, delivery, and measurement with a single-pass cell

The sampling set up for O₃ generation and delivery is shown in Fig. 1c. Ozone was generated by flowing oxygen (O₂), between 1–50 standard cm³ min⁻¹ (SCCM) with a mass flow controller (Alicat Scientific, MC-20SSCM-D-DB15/5m), through a discharge source (OzoneLabs, OL80) capable of generating up to 2% O₃. The O₃ concentration was diluted by a controlled flow of 1.5 standard L min⁻¹ (SLPM) of He via a second mass flow controller (Alicat Scientific, MC-5SLPM-D-DB15/5m) to produce O₃ concentrations in the range of 1.2×10^{15} – 2.4×10^{16} molecules cm⁻³ (58–1178 parts per million (ppm)). All experiments were conducted using a bath gas of He, which has a much smaller Rayleigh scattering cross section than nitrogen (N₂) or O₂ (Bodhaine et al., 1999) providing lower loss cavities with longer effective path lengths and higher sensitivity to optical absorption. Zero air and O₂ were avoided as bath gases due to the formation of O₄ (Greenblatt et al., 1990), which is observable with the IB-BCEAS instrument in the 350–470 nm region. The O₄ absorption associated with the small concentration of O₂ resulting from the dilution of the flow from the discharge source provided a negligible absorption interference as described below. A combination of a second mass flow controller and scroll pump controlled a 1.0 SLPM flow of gases through the IB-BCEAS. The excess flow of approximately 0.5 SLPM was vented to the atmosphere to maintain near-ambient pressure during all experiments. Instrument zeros consisted of a spectrum of He and were recorded by diverting the small flow of O₃ in O₂ from the discharge source to the exhaust using a three way valve. The experiment was not affected by turbulence because the flow was laminar, with a calculated Reynolds number of 13 (1.5 SLPM of He in a 2.2 cm diameter tube), and because He has a small refractive index which would minimize any optical effects due to turbulence.

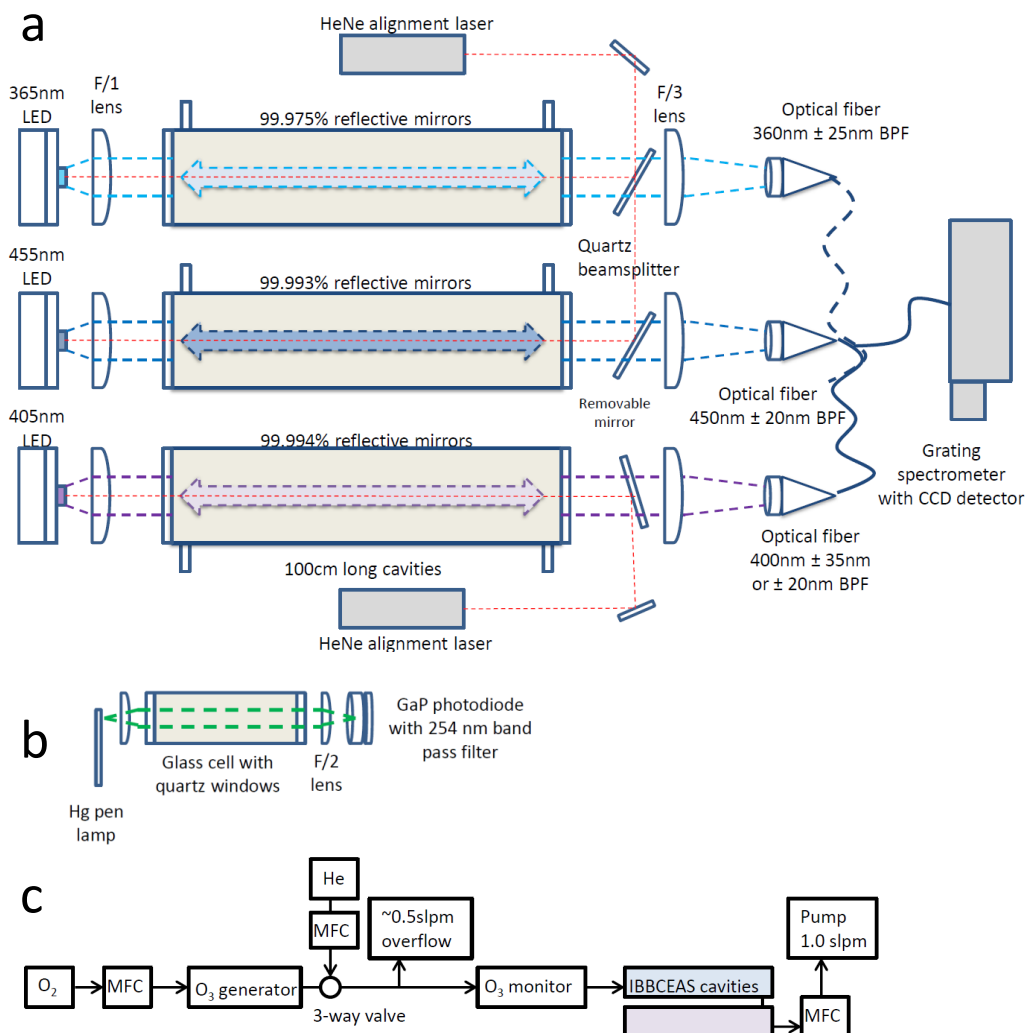


Fig. 1. (a) Schematic of the three channel IBBCEAS consisting of LED light sources, optical cavities, and a CCD detector. (b) Schematic of the ozone monitor, consisting of Hg light source and GaP photodiode. (c) Block diagram showing O₃ delivery system to the IBBCEAS.

Ozone concentrations were measured simultaneously with the IBBCEAS spectral measurements using a single-pass absorption measurement at 254 nm that consisted of a 10.6 cm glass cell with quartz windows, a mercury pencil lamp (UVP 90-0012-01), and gallium phosphide (GaP) photodiode detector (Thorlabs SM05PD7A) with a 254 nm band pass filter (Fig. 1b). The intensity of the photodiode was measured using an analog to digital interface (Measurement Computing USB-1408FS) and recorded in the data acquisition software. A dark background of the GaP photodiode was first taken to determine its internal noise (i). Following this, the diode signal was recorded for each of the He blanks (I_0) and each of the O₃ spectra (I). The signal was then averaged and Eq. (1) was used to determine the O₃ concentration, where d is the length of the absorption cell and the O₃ cross section, $\sigma_{\text{O}_3} = 1.141 \times 10^{-17} \text{ cm}^2 \text{ molecule}^{-1}$ at 253.7 nm, was taken from Orphal (2003).

$$[\text{O}_3] = \frac{\ln\left(\frac{I_0 - i}{I - i}\right)}{(d \times \sigma)} \quad (1)$$

The quoted uncertainty in the literature O₃ absorption cross section is 0.9% (Orphal, 2003). Our reported absorption cross section at 350–470 nm scales directly with the choice of cross section at 253.7 nm. The O₃ measurement was validated against a UV photometric O₃ instrument (Thermo Electron Corp., Model 49i, 102474-00) over the range of 50–165 ppm O₃ and the two agreed to within 1.0%, with a slope of 1.01 ± 0.01 and $r^2 = 0.9995$. Thus, we anticipate error on the order of 2% for the determination of the O₃ concentration itself.

2.3 Consideration of O₄ interference

As noted in the previous section, collision induced oxygen dimers, or O₄, absorb in the UV and visible spectral regions

(Greenblatt et al., 1990), and are a potential spectroscopic interference for measurement of weak O₃ absorptions. The O₂/O₃ flow from the discharge source was diluted with He (Fig. 1b), such that only up to 3.3% of flow through the IBBCEAS cells was from the O₃ source, of which, at most 1.8% could consist of O₄. Using Greenblatt et al. (1990) cross sections for O₄ of 4.1×10^{-46} , 2.4×10^{-46} , and 0.57×10^{-46} cm⁵ molecules⁻² at 360.5, 380.2, and 446.7 nm respectively and our experimental temperature and pressure, we calculated the expected O₄ optical density. For a maximum O₄ number density of 3.7×10^{17} molecules cm⁻³, the corresponding optical extinctions, α_{O_4} , are 5.6×10^{-11} , 3.3×10^{-11} , and 7.4×10^{-12} cm⁻¹ at 360.5, 380.2, and 446.7 nm, respectively. These optical extinctions are more than five orders of magnitude smaller than those that would be observed for O₃ at the same concentration and therefore, any O₄ interferences were considered negligible.

2.4 Operation of IBBCEAS instrument

The IBBCEAS instrument required approximately 30 min of warm up to allow the temperature of the LEDs, O₃ generator, and spectrometer to stabilize. Dark background spectra were acquired to correct for the pixel-dependent dark signal. These were scaled to the integration time and subtracted from subsequent sample spectra. Absolute measurement of optical extinction by IBBCEAS requires calibration of the mirror reflectivity, or alternatively, total cavity loss. For our apparatus, this calibration is based on Rayleigh scattering cross sections of pure gases. Following the acquisition of the dark background, spectra of He (I_{He}) and N₂ (I_{N_2}) were taken to determine the mirror reflectivity associated with each of the IBBCEAS cavities using Eq. (2) (Washenfelter et al., 2008).

$$\frac{1 - R(\lambda)}{d} = \frac{\left(\frac{I_{N_2}}{I_{He}}\right) \alpha_{Ray}^{N_2} - \alpha_{Ray}^{He}}{1 - \frac{I_{N_2}}{I_{He}}} \quad (2)$$

The Rayleigh scattering cross sections (σ_{Ray}) were taken from Bodhaine et al. (1999) and analysis of the spectra was done using Eqn. (3) (Washenfelter et al., 2008). The factor $(1 - R(\lambda))/d$, where d is the cavity length, was used directly from this calibration to derive concentrations rather than the mirror reflectivity itself. The Rayleigh scattering calibrations are accurate to within 3%. This accuracy is based on the $\pm 3\%$ accuracy of the Rayleigh N₂ cross sections compared to the measured values (Naus and Ubachs, 2000; Sneep and Ubachs, 2005) and the 3% repeatability of successive reflectivity measurements. The uncertainty of the Rayleigh scattering cross section for He is similar, but makes a minor contribution to the total uncertainty. Example spectra and calculated reflectivities are shown in Fig. 2.

Following calibration of total cavity loss, spectra of O₃ in He ($I(\lambda)$) at various concentrations were acquired alternately with spectra of pure He ($I_0(\lambda)$). Optical extinction due to O₃

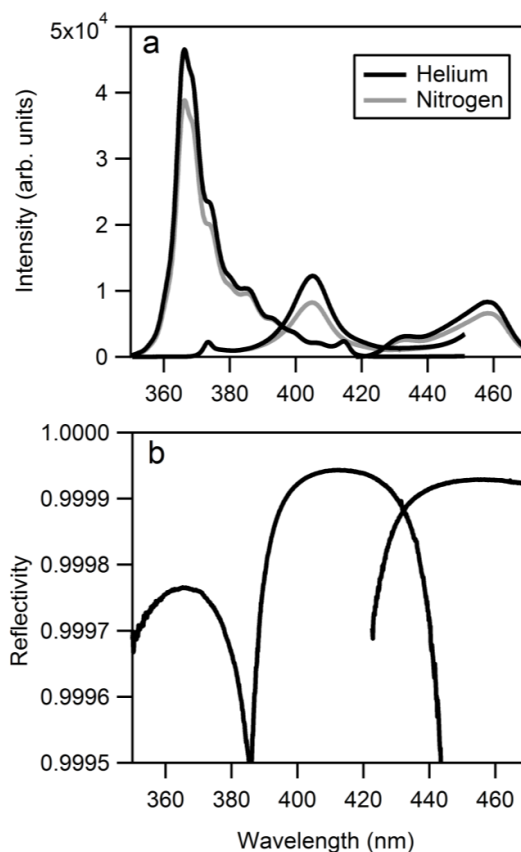


Fig. 2. (a) Example spectra of the transmitted intensity of He and N₂ through the 365, 405, and 455 nm IBBCEAS cavities. The structure observed for the 365 nm channel is due to the etalon structures from the 365 nm LED. (b) The derived reflectivity curves of the 365, 405, and 455 nm centered mirrors from Eq. (2).

(the product of number density and cross section) was then determined as follows.

$$\alpha_{abs}(\lambda) = [O_3] \sigma_{O_3} = \left(\frac{1 - R(\lambda)}{d} + \alpha_{Ray} \right) \left(\frac{I_0(\lambda) - I(\lambda)}{I(\lambda)} \right) \quad (3)$$

Spectra were integrated for 1.5 s and the average of 180 spectra was recorded. The optimum integration time for the O₃ spectra between successive zeros in He was determined from an Allan deviation analysis which measures the stability of the measurement, due to noise, over time (Fig. 3a). It was determined that alternating 5 min He and O₃ spectra, at or just beyond the minimum in the Allan deviation plot, was optimal. The stability of the optical cavity alignment itself was most likely responsible for the upward trend in the Allan deviation plot after 5 min since independent tests of the stability of the LEDs by a separate photodiode showed its output to be stable over a longer period of time (Fig. 3b). Similar to the reflectivity spectra, O₃ spectra were integrated for 1.5 s and 180 spectra were averaged.

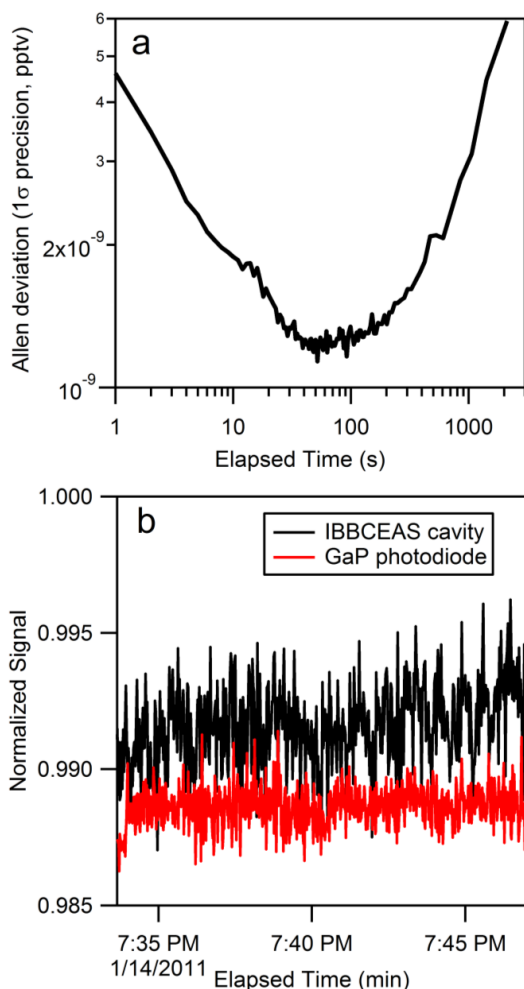


Fig. 3. (a) Allan deviation plot of the optical density of the IB-BCEAS for a single pixel at 370 nm in the 365 nm channel. The minimum near 5 min, was selected as the optimum sampling time between zeros. (b) Stability of the 365 nm LED intensity measured using a GaP photodiode, shown together with the stability of the IB-BCEAS cavities for a single pixel at 376 nm.

The O_3 spectrum from this work was obtained by averaging roughly one hour of O_3 spectra recorded simultaneously for the 365 nm and 405 nm cavities or the 405 nm and 455 nm cavities.

3 Results and discussion

3.1 Absolute absorption cross section of O_3

Fig. 4 shows the O_3 absorption cross section measured at 295 K and 820 hPa, together with previously measured cross sections (Burkholder and Talukdar, 1994; Brion et al., 1998; Burrows et al., 1999a; Voigt et al., 2001; Bogumil et al., 2003; Fuchs et al., 2009; Chen and Venables, 2011) obtained from the Mainz Spectral Database (Keller-Rudek and

Moortgat, 2011) and plotted for vacuum wavelengths. The Burkholder et al. (1994), Fuchs et al. (2009), and Chen and Venables (2011) spectra were corrected from air to vacuum wavelength using Eq. (1) in Ciddor (1996). The wavelength scale reported by Brion et al. (1998) is not specified. In our work, there were two sets of 405 nm spectra taken for the simultaneous measurement of the 365 nm and 405 nm cavities and the 405 nm and 455 nm cavities. Different band pass filters were used for the 405 nm cavity in each measurement to prevent out-of-band light from saturating the CCD detector. The sections were averaged in the wavelength regions where they overlap, and the final assembled spectrum is shown.

Plots of the optical extinction for single CCD pixels measured at various concentrations (Fig. 5) were used to compare the derived absorption cross sections to the experimental absorption cross sections seen in Fig. 4, and to test the linearity of the IB-BCEAS response over a range larger than one order of magnitude in O_3 . The cross sections determined from Fig. 4 are $\sigma_{O_3} = 3.87 \times 10^{-23} \text{ cm}^2$ at 365.0 nm, $\sigma_{O_3} = 1.47 \times 10^{-23} \text{ cm}^2$ at 405.0 nm, and $\sigma_{O_3} = 1.86 \times 10^{-22} \text{ cm}^2$ at 455.0 nm.

From the slope and slope uncertainty in Fig. 5, we calculate precisions for the 365, 405, and 455 nm channels of 2.3, 0.7, and 0.5 % respectively. Similar linear fits for spectra acquired with the 365 nm channel at 380 nm and 390 nm near the absorption minimum, have precisions of 3.1 % and 2.4 %, respectively. The absolute accuracy is calculated to be 4 % from quadrature addition of the uncertainties in the reflectivity (± 3 %), O_3 concentration (± 2 %), pressure (± 0.5 %), and temperature (± 0.7 %). However, the absolute accuracy can also be evaluated by comparing the cross section differences where the spectral channels overlap. At 386–387 nm, near the minimum, observed discrepancies of $1\text{--}2 \times 10^{-24} \text{ cm}^2$ between the 365 nm channel and two 405 nm channels are equivalent to an absolute accuracy of ~ 30 %, but this improves to less than 5 % at 395–424 nm for the two 405 nm channel measurements, and is 3–10 % at 424–442 nm in the overlap between the 405 nm and 455 nm channels.

In this very weakly absorbing region between the Huggins and Chappuis bands, there is more than an order of magnitude difference in the various reported O_3 cross sections (Brion et al., 1998; Burrows et al., 1999a; Voigt et al., 2001; Bogumil et al., 2003). Our reported spectrum agrees quantitatively with prior literature values at the edges of the spectrum. Our measurements are consistent most with Brion et al. (1998) with the exception of the minimum region from 375–390 nm, where our absorption cross section shows a lower minimum, but agrees within the combined uncertainty. Our measurements are also very consistent with those of Chen and Venables (2011), but their measurements do not extend past 375 nm. In addition, more defined O_3 structural features were observed in this work, Brion et al. (1998), and Chen and Venables (2011) when compared to the other literature cross sections (Burrows et al., 1999a; Voigt et al., 2001; Bogumil et al., 2003). The measurements also agree within

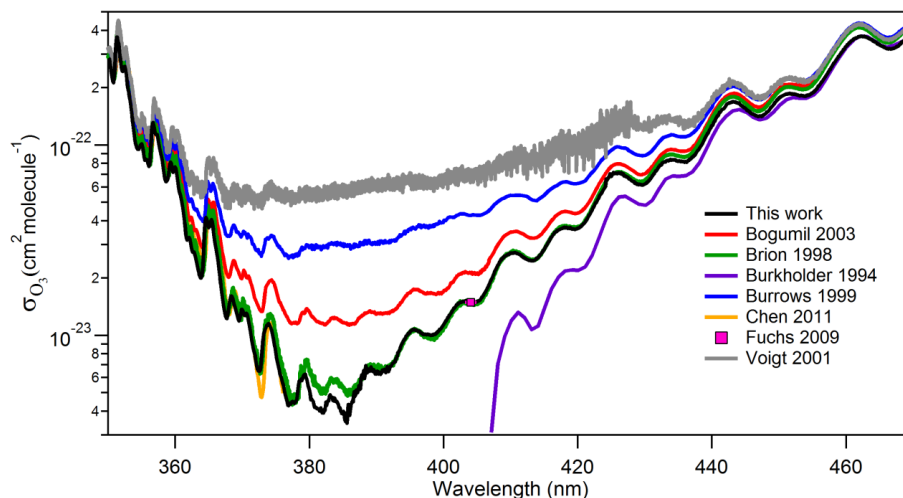


Fig. 4. The O_3 cross section from 350–470 nm determined in this work compared to other published measurements.

0.5 % at 404 nm with Fuchs et al. (2009), in which CRDS was used to measure the O_3 cross section, with the highest precision currently available within this wavelength range, to quantify its interference associated with measurements of NO_2 at the single wavelength of a diode laser.

Though the O_3 cross sections derived in this work agree best with the data of Brion et al. (1998), there is some disagreement between their spectra and ours near the minimum absorption at 375–390 nm. This is the region where the largest discrepancies have been reported. Prior to the measurements in this work, the lowest reported O_3 cross section were those of Brion et al. (1998) at 377.5 nm with a $\sigma_{\text{O}_3} = 4.4 \times 10^{-24} \text{ cm}^2$ and a reported uncertainty of 4 % near the absorption minimum. Chen and Venables (2011) examined the near-UV region from 335–375 nm, just to the short wavelength side of the minimum. These authors suggested that the absorption cross section in this region would be even lower than seen in previous studies (Brion et al., 1998; Burrows et al., 1999a; Voigt et al., 2001; Bogumil et al., 2003; Chen and Venables, 2011). In this work, the minimum was observed to be lower than the Brion et al. (1998) value, at 385.6 nm with $\sigma_{\text{O}_3} = 3.4 \times 10^{-24} \text{ cm}^2$, although the two measurements are consistent within their combined uncertainty.

3.2 Pressure and relative humidity effect on O_3

It has been suggested that O_3 cross sections could be sensitive to the molecular environment (Vaida et al., 1989; Frost and Vaida, 1995; Vaida and Headrick, 2000; Vaida, 2011). At the low partial pressures of O_3 used, ranging from 1.2×10^{15} – 2.4×10^{16} molecules cm^{-3} , there was no evidence of nonlinear O_3 partial pressure dependence as shown by Fig. 5. Spectroscopic and theoretical studies of the ozone dimer (Slanina and Adamowicz, 1993; Bahou et al., 2001; Probst et al., 2002; Sander et al., 2006) indicate the ozone dimer photoly-

sis cross section is much smaller than that of the monomer, and recent molecular beam studies by Chen et al. (2011) show the weak intermolecular interactions are not strong enough to affect the absorption spectra of the monomer. In addition, Orphal (2003) notes in his review that there is no experimental or theoretical evidence of pressure dependence in the O_3 cross section in the region of interest.

Spectroscopic and photofragment experiments (Hurwitz and Naaman, 1995) report increased OH formation from O_3 photolysis in the presence of water. This increase could be due to stronger absorption of radiation in the region between 350 and 470 nm by $\text{O}_3 \cdot \text{H}_2\text{O}$ complexes than by monomeric ozone (Frost and Vaida, 1995; Vaida, 2009; Vaida, 2011). These complexes have been detected experimentally (Schriver et al., 1990; Gillies et al., 1991; Tsuge et al., 2007). Limited information is available from matrix isolation studies about the UV spectra and photochemistry of the $\text{O}_3 \cdot \text{H}_2\text{O}$ complex (Leu, 1988; Jaeger, 1991; Dlugokencky and Ravishankara, 1992; King et al., 1994; Brasseur and Solomon, 1997; Langenberg and Schurath, 1999; Sennikov et al., 2005; Schriver et al., 1989).

With the IBBCEAS instrument, we attempted to observe the change in cross section of O_3 using relative humidities (RH) of up to 90 %. We did not observe any changes in the O_3 absorption spectrum due to the presence of water. This indicates that the product of the cluster number density and its cross section at the wavelengths of interest here is below the signal to noise of the experiment, which was less than 5 % at most wavelengths, passed on the precision of our measurements.

We can estimate upper limits for the cross section of the $\text{O}_3 \cdot \text{H}_2\text{O}$ complex in the wavelength region between 350 and 470 nm based on this result. Measured binding energies of the $\text{O}_3 \cdot \text{H}_2\text{O}$ complex range from -0.7 to $-2.4 \text{ kcal mol}^{-1}$ (Gillies et al., 1991). This translates to an equilibrium

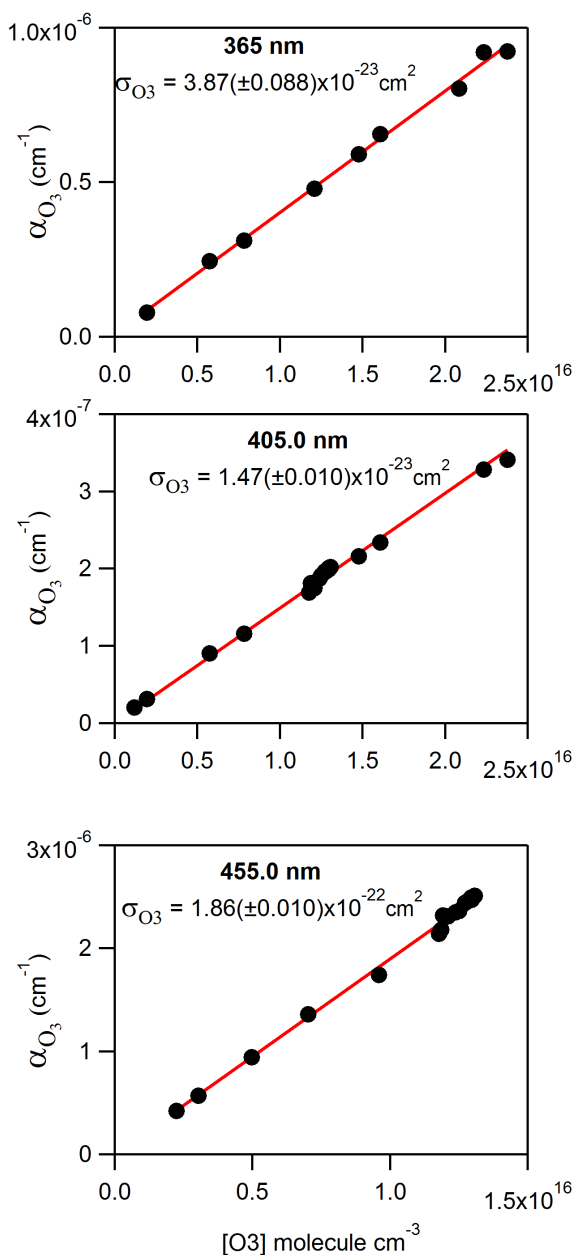


Fig. 5. Optical extinction measurements at various O_3 concentrations whose slope is the absolute absorption cross sections.

constant between $1.84 \times 10^{-4} \text{ atm}^{-1}$ and $3.55 \times 10^{-4} \text{ atm}^{-1}$ at room temperature (Frost and Vaida, 1995). At a relative humidity of 90 %, the ratio of $\text{O}_3 \cdot \text{H}_2\text{O} : \text{O}_3$ will be between 5.0×10^{-6} and 9.65×10^{-5} based on the equilibrium constants given above. This gives an upper limit for the enhancement in the absorption cross section of 1.0×10^4 or 5.0×10^{-2} for binding energies of -0.7 to $-2.4 \text{ kcal mol}^{-1}$, respectively.

4 Conclusions

Using a newly developed, high sensitivity IBBCEAS instrument, we measured the O_3 absolute absorption cross section from 350–470 nm at 295 K and 820 hPa with low O_3 partial pressures. These measurements directly address the large discrepancy in current literature cross sections in this region and agree well with the most recent measurements that are based on cavity enhanced methods which measured a portion of this spectral region. The effect of ozone concentration and relative humidity were investigated without any effect observed on the absorption cross section of O_3 . The absorption cross sections obtained here may be useful for applications such as satellite retrievals, ground-based O_3 monitoring, and atmospheric radiative transfer models. Future work may include temperature dependent measurements, since the O_3 cross section across this minimum is known to be strongly temperature dependent.

Acknowledgements. We thank Rich McLaughlin for machining custom mirror mounts for the IBBCEAS instrument. We thank Steve Ciciora for designing custom DC power supplies and amplifiers. All authors acknowledge funding from CIRES Innovative Research Program. JLA acknowledges support from the NASA Earth and Space Science Fellowship. VV acknowledges funding from NSF CHE 1011770. CJY and TFK thank NSERC for PDF scholarships.

Edited by: J. Abbatt

References

- Bahou, M., Schriver-Mazzuoli, L., and Schriver, A.: Infrared spectroscopy and photochemistry at 266 nm of the ozone dimer trapped in an argon matrix, *J. Chem. Phys.*, 114, 4045–4052, 2001.
- Bodhaine, B. A., Wood, N. B., Dutton, E. G., and Slusser, J. R.: On Rayleigh optical depth calculations, *J. Atmos. Ocean. Technol.*, 16, 1854–1861, 1999.
- Bogumil, K., Orphal, J., Homann, T., Voigt, S., Spietz, P., Fleischmann, O. C., Vogel, A., Hartmann, M., Kromminga, H., Bovensmann, H., Frerick, J., and Burrows, J. P.: Measurements of molecular absorption spectra with the SCIAMACHY pre-flight model: Instrument characterization and reference data for atmospheric remote-sensing in the 230–2380 nm region, *J. Photochem. Photobiol. A-Chem.*, 157, 167–184, 2003.
- Brasseur, G. and Solomon, S.: *Aeronomy of the Middle Atmosphere*, 3rd ed., D. Reidel, Dordrecht, The Netherlands, 401–442, 1997.
- Brion, J., Chakir, A., Daumont, D., Malicet, J., and Parisse, C.: High-resolution laboratory absorption cross-section of O_3 – Temperature effect, *Chem. Phys. Lett.*, 213, 610–612, 1993.
- Brion, J., Chakir, A., Charbonnier, J., Daumont, D., Parisse, C. and Malicet, J.: Absorption spectra measurements for the ozone molecule in the 350–830 nm region, *J. Atmos. Chem.*, 30, 291–299, 1998.

- Brown, S. S., Wilson, R. W., and Ravishankara, A. R.: Absolute intensities for third and fourth overtone absorptions in HNO_3 and H_2O_2 measured by cavity ring down spectroscopy, *J. Phys. Chem. A*, 104, 4976–4983, 2000.
- Burkholder, J. B. and Talukdar, R. K.: Temperature-dependence of the ozone absorption-spectrum over the wavelength range 410 to 760 nm, *Geophys. Res. Lett.*, 21, 581–584, 1994.
- Burrows, J. P., Richter, A., Dehn, A., Deters, B., Himmelmann, S., and Orphal, J.: Atmospheric remote-sensing reference data from GOME – Part 2. Temperature-dependent absorption cross sections of O_3 in the 231–794 nm range, *J. Quant. Spectrosc. Radiat. Transf.*, 61, 509–517, 1999a.
- Burrows, J. P., Weber, M., Buchwitz, M., Rozanov, V., Ladstätter-Weissenmayer, A., Richter, A., DeBeek, R., Hoogen, R., Bramstedt, K., Eichmann, K. U., and Eisinger, M.: The global ozone monitoring experiment (GOME): Mission concept and first scientific results, *J. Atmos. Sci.*, 56, 151–175, 1999b.
- Chen, I.-C., Chen, A. F., Huang, W.-T., Takahashi, K., and Lin, J. J.: Photolysis cross section of ozone dimer, *Chem Asian J.*, 6, 2925–2930, doi:10.1002/asia.201100526, 2011.
- Chen, J. and Venables, D. S.: A broadband optical cavity spectrometer for measuring weak near-ultraviolet absorption spectra of gases, *Atmos. Meas. Tech.*, 4, 425–436, doi:10.5194/amt-4-425-2011, 2011.
- Ciddor, P. E.: Refractive index of air: New equations for the visible and near infrared, *Appl. Optics*, 35, 1566–1573, 1996.
- Dlugokencky, E. J. and Ravishankara, A. R.: Laboratory measurements of direct ozone loss on ice and doped-ice surfaces, *Geophys. Res. Lett.*, 19, 41–44, 1992.
- Dube, W. P., Brown, S. S., Osthoff, H. D., Nunley, M. R., Ciciora, S. J., Paris, M. W., McLaughlin, R. J., and Ravishankara, A. R.: Aircraft instrument for simultaneous, in situ measurement of NO_3 and N_2O_5 via pulsed cavity ring-down spectroscopy, *Rev. Sci. Instrum.*, 77, 034101, doi:10.1063/1.2176058, 2006.
- Fiedler, S. E., Hese, A., and Ruth, A. A.: Incoherent broad-band cavity-enhanced absorption spectroscopy, *Chem. Phys. Lett.*, 371, 284–294, 2003.
- Frost, G. J. and Vaida, V.: Atmospheric implications of the photolysis of the ozone-water weakly bound complex, *J. Geophys. Res.-Atmos.*, 100, 18803–18809, 1995.
- Fuchs, H., Dube, W. P., Lerner, B. M., Wagner, N. L., Williams, E. J., and Brown, S. S.: A sensitive and versatile detector for atmospheric NO_2 and NO_x based on blue diode laser cavity ring-down spectroscopy, *Environ. Sci. Technol.*, 43, 7831–7836, 2009.
- Gherman, T., Venables, D. S., Vaughan, S., Orphal, J., and Ruth, A. A.: Incoherent broadband cavity-enhanced absorption spectroscopy in the near-ultraviolet: Application to HONO and NO_2 , *Environ. Sci. Technol.*, 42, 890–895, 2008.
- Gillies, J. Z., Gillies, C. W., Suenram, R. D., Lovas, F. J., Schmidt, T., and Cremer, D.: A microwave spectral and ab initio investigation of $\text{O}_3\text{-H}_2\text{O}$, *J. Mol. Spectrosc.*, 146, 493–512, 1991.
- Gratien, A., Picquet-Varrault, B., Orphal, J., Doussin, J. F., and Flaud, J. M.: New laboratory intercomparison of the ozone absorption coefficients in the mid-infrared (10 μm) and ultraviolet (300–350 nm) spectral regions, *J. Phys. Chem. A*, 114, 10045–10048, 2010.
- Greenblatt, G. D., Orlando, J. J., Burkholder, J. B., and Ravishankara, A. R.: Absorption measurements of oxygen between 330 nm and 1140 nm, *J. Geophys. Res.-Atmos.*, 95, 18577–18582, 1990.
- Hurwitz, Y. and Naaman, R.: Production of OH by dissociating ozone water complexes at 266 nm and 355 nm by reacting $\text{O}(^1\text{D})$ with water dimers, *J. Chem. Phys.*, 102, 1941–1943, 1995.
- Jaeger, K.: Ph.D. Thesis, University of Bremen, Germany, 111–136, 1991.
- Keller-Rudek, H. and Moortgat, G. K.: MPI-Mainz-UV-VIS Spectral Atlas of Gaseous Molecules, www.atmosphere.mpg.de/spectral-atlas-mainz, 1 August 2011.
- King, D. S., Sauder, D. G., and Casassa, M. P.: Cluster effects in $\text{O}_3/\text{H}_2\text{O}$ Photochemistry: Dynamics of the $\text{O}+\text{H}_2\text{O}\rightarrow 2\text{OH}$ reaction photoinitiated in the $\text{O}_3\text{H}_2\text{O}$ dimer, *J. Chem. Phys.*, 100, 4200–4210, 1994.
- Kroon, M., de Haan, J. F., Veefkind, J. P., Froidevaux, L., Wang, R., Kivi, R., and Hakkarainen, J. J.: Validation of operational ozone profiles from the Ozone Monitoring Instrument, *J. Geophys. Res.-Atmos.*, 116, D18305, doi:10.1029/2010JD015100, 2011.
- Langenberg, S. and Schurath, U.: Ozone destruction on ice, *Geophys. Res. Lett.*, 26, 1695–1698, 1999.
- Langridge, J. M., Ball, S. M., and Jones, R. L.: A compact broadband cavity enhanced absorption spectrometer for detection of atmospheric NO_2 using light emitting diodes, *Analyst*, 131, 916–922, 2006.
- Langridge, J. M., Ball, S. M., Shillings, A. J. L., and Jones, R. L.: A broadband absorption spectrometer using light emitting diodes for ultrasensitive, in situ trace gas detection, *Rev. Sci. Instrum.*, 79, 123110, 2008.
- Leu, M. T.: Heterogeneous reactions of N_2O_5 with H_2O and HCl on ice surfaces – implications for Antarctic ozone depletion, *Geophys. Res. Lett.*, 15, 851–854, 1988.
- Matthews, J., Sinha, A., and Francisco, J. S.: The importance of weak absorption features in promoting tropospheric radical production, *Proc. Natl. Acad. Sci. USA*, 102, 7449–7452, 2005.
- Naus, H. and Ubachs, W.: Experimental verification of Rayleigh scattering cross sections, *Opt. Lett.*, 25, 347–349, 2000.
- Orphal, J.: A critical review of the absorption cross-sections of O_3 and NO_2 in the ultraviolet and visible, *J. Photochem. Photobiol. A-Chem.*, 157, 185–209, 2003.
- Petrovavlovskikh, I., Evans, R., McConville, G., Oltmans, S., Quincy, D., Lantz, K., Disterhoft, P., Stanek, M., and Flynn, L.: Sensitivity of Dobson and Brewer Umkehr ozone profile retrievals to ozone cross-sections and stray light effects, *Atmos. Meas. Tech.*, 4, 1841–1853, doi:10.5194/amt-4-1841-2011, 2011.
- Probst, M., Hermansson, K., Urban, J., Mach, P., Muigg, D., Denifl, G., Fiegele, T., Mason, N. J., Stamatovic, A., and Mark, T. D.: Ionization energy studies for ozone and OCIO monomers and dimers, *J. Chem. Phys.*, 116, 984–992, 2002.
- Sander, S. P., Finlayson-Pitts, B. J., Friedl, B. J., Golden, D. M., Huie, R. E., Keller-Rudek, H., Kolb, C. E., Kurylo, M. J., Molina, M. J., Moortgat, G. K., Orkin, V. L., Ravishankara, A. R., and Wine, P. H.: Chemical Kinetics and Photochemical Data for Use in Atmospheric Studies 06-2, Jet Propulsion Laboratory, Pasadena, CA, USA, 2006.
- Sansonetti, C. J., Salit, M. L., and Reader, J.: Wavelengths of spectral lines in mercury pencil lamps, *Appl. Optics*, 35, 74–77, 1996.
- Schrivver, A., Schriver, L., Barreau, C., Carrire, D., Perchard, J. P., Jaeger, K., and Schrems, O.: Ozone in the Atmosphere: Pro-

- ceedings of the Quadrennial Ozone Symposium 1988 and Tropospheric Ozone Workshop, A. Deepak Publishing, 694–697, 1989.
- Schrivver, L., Barreau, C., and Schriver, A.: Infrared spectroscopic and photochemical study of water ozone complexes in solid argon, *Chem. Phys.*, 140, 429–438, 1990.
- Sennikov, P. G., Ignatov, S. K., and Schrems, O.: Complexes and clusters of water relevant to atmospheric chemistry: H₂O complexes with oxidants, *Chem. Phys. Chem.*, 6, 392–412, 2005.
- Slanina, Z. and Adamowicz, L.: Computational studies of atmospheric chemistry species. 3. A computational study of the ozone dimer, *J. Atmos. Chem.*, 16, 41–46, 1993.
- Sneep, M. and Ubachs, W.: Direct measurement of the Rayleigh scattering cross section in various gases, *J. Quant. Spectrosc. Radiat. Transf.*, 92, 293–310, 2005.
- Thalman, R. and Volkamer, R.: Inherent calibration of a blue LED-CE-DOAS instrument to measure iodine oxide, glyoxal, methyl glyoxal, nitrogen dioxide, water vapour and aerosol extinction in open cavity mode, *Atmos. Meas. Tech.*, 3, 1797–1814, doi:10.5194/amt-3-1797-2010, 2010.
- Tsuge, M., Tsuji, K., Kawai, A., and Shibuya, K.: Infrared spectroscopy of ozone-water complex in a neon matrix, *J. Phys. Chem. A*, 111, 3540–3547, 2007.
- Vaida, V.: Spectroscopy of photoreactive systems: Implications for atmospheric chemistry, *J. Phys. Chem. A*, 113, 5–18, 2009.
- Vaida, V.: Perspective: Water cluster mediated atmospheric chemistry, *J. Chem. Phys.*, 135, 1–8, 2011.
- Vaida, V. and Headrick, J. E.: Physicochemical properties of hydrated complexes in the Earth's atmosphere, *J. Phys. Chem. A*, 104, 5401–5412, 2000.
- Vaida, V., Donaldson, D. J., Strickler, S. J., Stephens, S. L., and Birks, J. W.: A reinvestigation of the electronic-spectra of ozone condensed-phase effects, *J. Phys. Chem.*, 93, 506–508, 1989.
- Vaughan, S., Gherman, T., Ruth, A. A., and Orphal, J.: Incoherent broad-band cavity-enhanced absorption spectroscopy of the marine boundary layer species I₂, IO and OIO, *Phys. Chem. Chem. Phys.*, 10, 4471–4477, 2008.
- Venables, D. S., Gherman, T., Orphal, J., Wenger, J. C., and Ruth, A. A.: High sensitivity in situ monitoring of NO₃ in an atmospheric simulation chamber using incoherent broadband cavity-enhanced absorption spectroscopy, *Environ. Sci. Technol.*, 40, 6758–6763, 2006.
- Voigt, S., Orphal, J., and Burrows, J. P.: The temperature and pressure dependence of the absorption cross-sections of NO₂ in the 250–800 nm region measured by Fourier-transform spectroscopy, *J. Photochem. Photobiol. A-Chem.*, 149, 1–7, 2002.
- Voigt, S., Orphal, J., Bogumil, K., and Burrows, J. P.: The temperature dependence (203–293 K) of the absorption cross sections of O₃ in the 230–850 nm region measured by Fourier-transform spectroscopy, *J. Photochem. Photobiol. A-Chem.*, 143, 1–9, 2001.
- Waschewsky, G. C. G., Horansky, R., and Vaida, V.: Effect of dimers on the temperature-dependent absorption cross section of methyl iodide, *J. Phys. Chem.*, 100, 11559–11565, 1996.
- Washenfelder, R. A., Langford, A. O., Fuchs, H., and Brown, S. S.: Measurement of glyoxal using an incoherent broadband cavity enhanced absorption spectrometer, *Atmos. Chem. Phys.*, 8, 7779–7793, doi:10.5194/acp-8-7779-2008, 2008.